Atmos. Chem. Phys. Discuss., 14, 13963–14004, 2014
www.atmos-chem-phys-discuss.net/14/13963/2014/
doi:10.5194/acpd-14-13963-2014

Atmospheric Chemistry and Physics Discussions

Characteristics of trace metals in traffic-derived particles in Hsuehshan Tunnel, Taiwan: size distribution, fingerprinting metal ratio, and emission factor

Y.-C. Lin[1], C.-J. Tsai[2], Y.-C. Wu[3], R. Zhang[4], K.-H. Chi[5], Y.-T. Huang[1], S.-H. Lin[1], and S.-C. Hsu[1]

[1]Research Center for Environmental Changes, Academia Sinica, Nankang, Taipei, 115, Taiwan
[2]Institute of Environmental Engineering, National Chiao Tung University, Hsinchu, 300, Taiwan
[3]Environmental Analysis Laboratory, Environmental Protection Administration, Executive Yuan, 320, Taiwan
[4]Key Laboratory of Regional Climate-Environment Research for Temperate East Asia, Institute of Atmospheric Physics, Chinese Academy of Sciences, Beijing, China
[5]Institute of Environmental and Occupational Health Sciences, National Yang Ming University, Taipei 112, Taiwan

Received: 5 May 2014 – Accepted: 9 May 2014 – Published: 28 May 2014

Correspondence to: S.-C. Hsu (schsu815@rcec.sinica.edu.tw)
and Y.-C. Lin (yclin26@rcec.sinica.edu.tw)

Published by Copernicus Publications on behalf of the European Geosciences Union.

ACPD
14, 13963–14004, 2014

Abstract

Traffic emissions are a significant source of airborne particulate matter (PM) in ambient environments. These emissions contain high abundance of toxic metals and thus pose adverse effects on human health. Size-fractionated aerosol samples were collected from May to September 2013 by using micro-orifice uniform deposited impactor (MOUDI). Sample collection was conducted simultaneously at the inlet and outlet sites of Hsuehshan Tunnel in northern Taiwan, which is the second longest freeway tunnel (12.9 km) in Asia. Such endeavor aims to characterize the chemical constituents, size distributions, and fingerprinting ratios, as well as the emission factors of particulate metals emitted by vehicle fleets. A total of 36 metals in size-resolved aerosols were determined through inductively coupled plasma mass spectrometry. Three major groups, namely, tailpipe emissions (Zn, Pb, and V), wear debris (Cu, Cd, Fe, Ga, Mn, Mo, Sb, and Sn), and resuspended dust (Ca, Mg, K, and Rb), of airborne PM metals were categorized on the basis of the results of enrichment factor, correlation matrix, and principal component analysis. Size distributions of wear-originated metals resembled the pattern of crustal elements, which were predominated by super-micron particulates (PM_{1-10}). By contrast, tailpipe exhaust elements such as Zn, Pb, and V were distributed mainly in submicron particles. By employing Cu as a tracer of wear abrasion, several intermetal ratios, including Fe/Cu (14), Ba/Cu (1.05), Sb/Cu (0.16), Sn/Cu (0.10), and Ga/Cu (0.03), served as fingerprints for wear debris. Emission factor of PM_{10} mass was estimated to be 7.7 mg vkm^{-1}. The metal emissions were mostly predominated in super-micron particles (PM_{1-10}). Finally, factors that possibly affect particulate metal emissions inside Hsuehshan Tunnel are discussed.

ACPD
14, 13963–14004, 2014

1 Introduction

Traffic emissions are an important source of particulate matters (PM) (Sternbeck et al., 2002; Birmili et al., 2006; Lough et al., 2005; Johansson et al., 2009) in urban atmosphere. Exposure to traffic-derived PM poses adverse effects on human health and increases the risk of respiratory illness, cardiovascular diseases, and asthma (Brauer et al., 2002; Defino et al., 2005), resulting in increased mortality (Nel, 2005).

Airborne traffic-related PM is emitted mainly from tailpipe exhaust (exhaust emissions), wear from brake linings and tires, as well as re-suspension of road dust (non-exhaust emissions) by moving vehicles (Rogge et al., 1993; Cadle et al., 1999; Garg et al., 2000; Wåhlin et al., 2006; Lawrence et al., 2013). Exhaust emissions contribute a large amount of fine particulate matters (aerodynamic diameter less than 2.5 µm, $PM_{2.5}$), whereas non-exhaust emissions mainly consist of coarser particles (Abu-Allaban et al., 2002; Sanders et al., 2003). With regard to elemental compositions, Pb, Zn, Ni, and V in submicron particles were commonly attributed to pipe emissions and fuel oil combustion of gasoline and diesel engines (Lin et al., 2005; Wang et al., 2003; Shafer et al., 2012). Silicon (Si), Fe, Ca, Na, Mg, Al, and K are essentially found in coarser particles and are associated with re-suspension of road dust. Large amounts of Ca and K observed in submicron particles occasionally originate from the tailpipe emission of lubricating oil as well as the vaporization of volatile K-compounds and potassium titanate ($K_2O \cdot nTiO_2$), which is used for improving heat resistance and wear characteristics (Hee and Filip, 2005; Iijima et al., 2007; Kuo et al., 2009). Meanwhile, Cu, Ba, Sb, Fe, Cd, Cr, Ga, Sn, and Zn, which are commonly associated with wear dust from brake linings and tires, are predominant in coarse PM (Lough et al., 2005; Grieshop et al., 2006; Thorpe and Harrison, 2008). A number of studies investigated the chemical and physical properties of traffic-originated PM by performing conventional dynamometric tests and field measurements near roads and inside tunnels (Sternbeck et al., 2002; Sanders et al., 2003; Birmili et al., 2006; Wåhlin et al., 2006; Iijima et al., 2007; Harrison et al., 2012; Dall'Osto et al., 2013; Lawrence

ACPD
14, 13963–14004, 2014

et al., 2013). Dynamometric tests may allow optimal control of experimental conditions; however, such tests may inadequately reflect real-world traffic emissions. Field measurements nearby roadsides are insufficient to isolate the influence of other emission sources surrounding the sampling station, suggesting that tunnel measurement can more effectively address this issue.

Tunnel aerosol sampling is designed to explore size distributions, chemical compositions, and emission factors (EmF) of traffic-related aerosols and their associated compositions (Weingartner et al., 1997; Funasaka et al., 1998; Gillies et al., 2001; Sternbeck et al., 2002; Grieshop et al., 2006; Chiang and Huang, 2009; Pio et al., 2013). Pio et al. (2013) discriminated three main types of aerosols in Marquês tunnel, Portugal, namely, carbonaceous, soil component, and vehicle mechanical wear. They also suggested that Cu is a good tracer for wear emissions of road traffic. Wear emission elements such as Zn, Sb, and Ba exhibited a peak mode in the size range of 3.2 to 5.6 µm. In comparison, Pb, Ca, and Fe partitioned within 0.1 µm are mostly emitted from combustion of fuel and lubricant oil or vaporization from hot brake surface (Lough et al., 2005). Sternbeck et al. (2002) collected aerosol samples in two tunnels in Sweden and analyzed trace metals through inductively coupled plasma mass spectrometry (ICP-MS). They concluded that vehicle-related metals, such as Cu, Zn, Cd, Sb, Ba, and Pb, originated mainly from wear rather than from combustion, and that heavy-duty vehicles (HDV), rather than light-duty vehicles (LDV), are the leading emitter of Ba and Sb. They further suggested that a Sb/Cu ratio of ~ 0.22 indicates the presence of brake wear-related particles.

A series of aerosol sampling was conducted at two sites in Hsuehshan Tunnel by using micro-orifice uniform deposited impactors (MOUDI) to characterize the physical and chemical properties of metallic aerosols under real driving conditions. A total of 24 sets of size-resolved aerosol samples were collected; 36 trace metals were analyzed by ICP-MS. Elemental compositions, size distributions, and fingerprinting metal ratios in traffic aerosols are reported in this paper. The resulting comprehensive dataset would

ACPD
14, 13963–14004, 2014

provide useful insight into health effect studies, source apportionment of atmospheric metals, and emissions inventory of traffic-related particulate metals.

2 Methodology

2.1 Site description

With a length of 12.9 km, Hsuehshan Tunnel is the second longest road tunnel in Asia and the fifth longest in the world. Given its length and isolation from non-traffic sources, this tunnel is a suitable study area for the behaviors of air pollutants associated with vehicle fleets (Chang et al., 2009; Chen et al., 2010; Cheng et al., 2010a; Zhu et al., 2010; Li et al., 2011; Lai and Peng, 2012). Opened to traffic in June 2006, Hsuehshan Tunnel connects Pingling in New Taipei City and Toucheng in Yilan County. The tunnel has two separate two-lane bores and ascends steadily from 44 m a.m.s.l. (above mean sea level) at the south end (Toucheng) to 208 m a.m.s.l. at the north end (Pingling), that is, a slope of 1.26 %. Only passenger cars and light-duty trucks (which are both classified under LDV) as well as shuttle buses (categorized under HDV) are allowed to travel inside the tunnel with vehicle speed limited to 90 km.

A ventilation system composed of three air exchange stations and three air interchange stations was built inside the tunnel to maintain air quality. Exchange and interchange stations are located alternatively at an interval of nearly 2 km. In exchange stations, polluted air is exchanged with outer fresh air by using separate fresh and exhaust shafts equipped with two sets of fans. Fans are typically triggered at temperatures higher than 40 °C or CO concentrations higher than 75 ppm. At interexchange stations, the air in each bore is diverted into another bore by two sets of fans, which are also triggered when CO concentration exceeds 75 ppm.

ACPD
14, 13963–14004, 2014

2.2 Sampling and analysis

Four aerosol sampling campaigns were conducted between May and September 2013; each campaign lasted for three days: Friday to Sunday. During the sampling campaigns, two aerosol samplers were installed in the northbound bore and were placed at 1.7 and 10.6 km from the entrance. Thus, the distance between the inlet and outlet sites is 8.9 km. MOUDI (model 100, MSP Corporation, Minneapolis, Minnesota) equipped with pre-weighed Teflon filters (PTFE, 47 mm in diameter and 1.0 mm in pore size, Pall Gelman, East Hills, New York) were used to collect size-resolved aerosol samples. MOUDI consists of 10 size-fractionating stages with 50 % cut-off diameters of 10, 5.6, 3.2, 1.8, 1.0, 0.56, 0.32, 0.18, 0.10, and 0.056 µm, plus an inlet (nominal cut size of 18 µm) and an after-filter (< 0.018 µm) at the base. Flow rate was calibrated prior to each sampling run and maintained at 30 L min^{-1}. Each sample was collected for 12 h (typically from 9 a.m. to 9 p.m.) daily. After sampling, filter samples were conditioned for 48 h, followed by gravimetric measurement at 23 °C and RH 30 ± 5 % with a microbalance (METTLER TOLEDO, AX205, precision 1 µg) to determine the net mass of collected aerosol particles, which is needed to calculate the PM mass concentration. The samples were then subject to acid digestion with the use of an ultra-high throughput microwave digestion system (MARSXpress, CEM Corporation, Matthews, NC). The vessels were acid-cleaned thoroughly prior to sample digestion. A half of each sample filter was digested in an acid mixture (1.5 mL 60 % HNO_3 and 1.5 mL 48 % HF). After digestion, the vessels were transferred to the XpressVap™ accessory sets (CEM) for evaporation of the remaining acids. When nearly dried, 2 mL concentrated HNO_3 was added into each vessel and reheated. The resulting solution was then diluted with Milli-Q water to a final volume of 15 mL for analysis. The digestion procedure has been detailed in previous studies (Hsu et al., 2008, 2009; Zhang et al., 2013).

A total of 36 target elements in aerosols were analyzed by ICP-MS (Elan 6100, Perkin Elmer™ SCIEX, USA). For each run, a blank reagent and three filter membrane blanks were subject to the same procedures as those for the samples. Indium (In) was

ACPD
14, 13963–14004, 2014

added to the digests as an internal standard with a final concentration of 10 ng mL^{-1} for ICP-MS analysis. The QA/QC of data is guaranteed by the analysis of a standard reference material, SRM 1648 (urban atmospheric particulate matter prepared by the National Institute Standards and Technology (NIST)). The recoveries of target elements mostly fell within 10 % ($n = 5$) of certified or reference values (Table S1). Table S1 also presents the method detection limits (MDLs) for the analyzed elements. Details of the ICP-MS analysis has been extensively described by Hsu et al. (2010) and Zhang et al. (2013).

2.3 Enrichment factor and principal component analysis

In addition to size distribution, three approaches, namely, enrichment factor (ErF), correlation matrix, and principal component analysis (PCA) were applied to explore the possible sources and associations of elements. ErF is used to assess the influence of crustal source on a given metal (X_i), which can be calculated by using the following equation:

$$\mathrm{ErF}(X_i) = \frac{(X_i/\mathrm{Al})_{\mathrm{PM}}}{(X_i/\mathrm{Al})_{\mathrm{Crust}}} \quad (1)$$

where $(X_i/\mathrm{Al})_{\mathrm{PM}}$ is the concentration ratio of a given element X to Al in tunnel particulate matters and $(X_i/\mathrm{Al})_{\mathrm{Crust}}$ is the concentration ratio of an interested element X to Al in the average crust abundance (Taylor, 1964).

PCA can elucidate variance in a given dataset in terms of minimum number of significant component. This technique has been employed in the tunnel studies concerning source apportionment of airborne metals (Lin et al., 2005; Lawrence et al., 2013). The software used here is STATISTICA 12 (Statsoft Inc.). A factor loading of > 0.7 was adopted in this study to assign source identification to a given principal component.

ACPD
14, 13963–14004, 2014

2.4 Emission factor estimation

The observed data are used to calculate emission factors (EmF, mg vkm^{-1} for PM, and µg vkm^{-1} for trace metals) for vehicle fleets under real driving conditions. The EmF for PM is calculated as follows (Pierson et al., 1996; Sternbeck et al., 2002):

$$\mathrm{EmF} = \frac{(C_o - C_i) \cdot V_{air}}{NL} \quad (2)$$

where C_o and C_i are the concentrations of observed PM at the outlet and inlet sites, respectively; V_{air} is the ventilation flow through the tunnel (m^3 s^{-1}); N is the traffic flow (vehicle s^{-1}), and L (km) is the distance between the inlet and outlet sites. V_{air} is calculated as product of wind speed (m s^{-1}) and the cross section area of the tunnel (56.6 m^2). L is 8.9 km, which is equivalent to the distance between two sites.

3 Result and discussions

3.1 Chemical compositions

Table 1 summarizes the data on PM mass concentrations in size-resolved aerosols at both the inlet and outlet sites in Hsuehshan Tunnel. The aerosols are treated into three size bins: submicron (PM_1), fine ($PM_{1-1.8}$), and coarse ($PM_{1.8-10}$) modes. During the sampling periods, the mass concentrations of PM_{10}, which were determined as the sum of aerosol masses at all corresponding stages with a cut-off diameter less than 10 µm, ranged from 35 to 67 µg m^{-3} (average: 54 ± 9 µg m^{-3}) at the inlet site and from 106 to 242 µg m^{-3} (average: 162 ± 42 µg m^{-3}) at the outlet site. Submicron particles were the predominant fraction, accounting for 60 ± 6 % and 82 ± 3 % of PM_{10} mass at the entrance and the exit, respectively. The abundance of submicron PM may indicate that combustion processes are significant sources of tunnel aerosols, which are presumably dominated by carbonaceous particles (Zhu et al., 2010; Pio et al., 2013). Another

ACPD
14, 13963–14004, 2014

plausible explanation is the absorption of organic gases by Teflon filters, thereby enhancing carbonaceous materials in submicron PM (Cabada et al., 2004). Compared with the inlet site, higher concentrations of $PM_{1-1.8}$ and PM_1 were observed at the outlet site by a factor of 2.5 and 4.4, respectively. The mean concentration of $PM_{1.8-10}$ at the outlet site was $17 \pm 4\,\mu g\,m^{-3}$, which is nearly equal to that ($18 \pm 5\,\mu g\,m^{-3}$) at the inlet site. This indicates that finer particles are relatively efficiently transported from the entrance to the exit; previous studies have attributed such efficient transport to "piston effect" (Chang et al., 2009; Cheng et al., 2010a; Moreno et al., 2014). These authors suggested that passing vehicles peak up air pollutants emitted from vehicle fleets and the flows lead them to the exit, resulting in the accumulation of large quantities of air pollutants in that area. The ratio of 4.4 might be regarded as a reference ratio of difference in PM mass between two sites caused by traffic emissions, and this value would hold for $PM_{1-1.8}$ and $PM_{1.8-10}$ if no significant removal occurred for super-micron PM (PM_{1-10}) during their travel. Therefore, only 2.5 was found for $PM_{1-1.8}$, indicating that $\sim 43\,\%$ of airborne $PM_{1-1.8}$ has been deposited out of the air by certain processes such as dry deposition to surface or adherence onto the tunnel wall. For $PM_{1.8-10}$, the concentration at the outlet site was nearly equal to that at the inlet site (outlet-to-inlet ratio: ~ 1.1), revealing that 75 % of coarse PM were removed during their transport downwind. The outlet-to-inlet ratio of PM mass concentrations increases with decreasing PM size, indicating that finer particles are transported toward the exit as a result of the "piston effect" in tunnels.

Figure 1a shows the average elemental concentrations of PM_{10} at the two sites in Hsuehshan Tunnel, and Fig. 1b depicts the partitioning of trace elements among three size bins. As shown in Fig. 1a, Fe was the most abundant element, with a mean concentration of $2384 \pm 1416\,ng\,m^{-3}$. In addition to Na, Ca, and Al (500 to $300\,ng\,m^{-3}$), Zn, K, Ba, Cu, and Mg (up to $100\,ng\,m^{-3}$) were also major metals in PM_{10}, followed by Ti ($73\,ng\,m^{-3}$), Mn ($29\,ng\,m^{-3}$), Sb ($23\,ng\,m^{-3}$), and then followed by Mo, Pb, Ga, Sr, Ni, V, and Ce (10 to $1\,ng\,m^{-3}$). The rest of the elements have concentrations less than $1\,ng\,m^{-3}$ (i.e., $0.9\,ng\,m^{-3}$ for Bi to $0.02\,ng\,m^{-3}$ for U). Most elements exhibited

ACPD
14, 13963–14004, 2014

significantly higher concentrations at the exit than at the entrance ($p < 0.05$, Fig. 1c), with the exception of a number of crustal elements such as Al, K, Mg, and Rb. This suggests that a lower road dust reservoir is present inside the freeway tunnel (Amato et al., 2012). Considerably high outlet-to-inlet ratios (ranging from 2.2 for Sr to 4.3 for Zn) were found for traffic-derived elements, including Zn, Cu, Ba, Mn, Sb, Sn, Pb, Ga, Sr, and Cd.

3.2 Size distributions

The average size distributions of some of the analyzed metals are shown in Figs. 1b, 2 and S1. Barium (Ba), Cd, Cu, Fe, Ga, Mn, Mo, Sb, and Sn were predominant in coarse mode at the entrance (Fig. 1b). These elements displayed a typical mono-modal distribution with a major peak in the size range of 3.2–5.6 µm, while they had another small peak at 1.0–1.8 µm at times (Figs. 2 and S2). The size distribution patterns of these metals were consistent with the results observed by Harrison et al. (2012) at a curbside in central London. The authors assigned the elements Fe, Cu, Sb, Ba, and Zn to the non-exhaust traffic particles. At the outlet site, those elements (Ba, Cd, Cu, Fe, Ga, Mn, Mo, Sb, and Sn) similarly had a mono-modal size distribution, but the main peak shifted to 1.0–1.8 µm (Figs. 2 and S2). Similar to that in PM, this shift was perhaps due to "piston effect," which, as previously mentioned, facilitated the transport of finer PM to the exit.

Zinc (Zn) showed a bi-modal distribution for most samples at the entrance, with a major peak in the size range of 3.2–5.6 µm and a second peak in the size range of 0.56–1.0 µm. Meanwhile, a mono-modal pattern with a major peak at 1.0–1.8 µm was found at the exit. Lead (Pb) displayed two peaks at the inlet site: one at 0.56–1.0 µm and another one at 3.2–5.6 µm. However, Pb exhibited a typical mono-modal distribution at the outlet site, peaking at 0.32–0.56 µm. Vanadium (V) revealed a bi-modal size pattern with a major peak at 0.32–0.56 µm and a second peak at 3.2–5.6 µm at the inlet site, whereas it peaked at 0.18–0.32 µm or 0.32–0.56 µm at the exit.

ACPD
14, 13963–14004, 2014

Aluminum (Al), Ca and Mg of predominant geological origins showed a typical mono-modal size distribution at the inlet site with a major peak at 3.2–5.6 µm; however, a peak was occasionally found in the submicron particles (Figs. S1 and S3). For example, the abundance of Al, Ca and K was observed at submicron size in two sets of samples (21 July and 10 August). Such abundance was ascribed to non-crustal sources such as vaporization from lubricating oil and diesel emissions (Wang et al., 2003), which perhaps alters the size distributions of these crustal elements. Submicron mode, which is an indicator of combustion or high temperature processes, contributes non-negligible Ca and K, which are usually regarded as crustal elements. Potassium titanate and a number of volatile compounds are known to contain K and therefore may be the possible sources of submicron K (Hee and Filip, 2005; Iijima et al., 2007). Submicron Ca probably originated from tailpipe emissions of lubricating oil (Kuo et al., 2009). Like traffic elements, these crustal elements had a major peak that shifted to 1.0–1.8 µm at the outlet site, which was also arisen from the "piston effect". At the inlet site, rare earth elements (REEs), such as La, Ce, Nd, Pr, and Sm, revealed a mono-modal size distribution with a major peak at 3.2–5.6 µm. At the exit, such elements essentially showed a mono-modal distribution that peaked at 1.0–1.8 µm.

3.3 Sources of trace metals

Figure 3 presents the results of enrichment factor analysis for all analyzed elements in three size bins of size-segregated particles at both the inlet and outlet sites. ErF values for all species were higher at the outlet than at the inlet site, suggesting that the influence of re-suspended road dust were insignificant for most metals at the exit. Enrichment factor values for Ca, K, Mg, Rb, Sr, and Ti in the three size-resolved particles were generally close to unity at both sites, demonstrating that these elements originated mainly from the resuspension of soil and road dust. ErF values for these geological metals increased with decreasing size, indicating that these elements in smaller particles would be significantly influenced by anthropogenic sources such as diesel emissions, lubricating oil, and additive in oil fuels. For lanthanides, lower enrich-

ACPD
14, 13963–14004, 2014

ment was found for La, Pr, Nd, and Sm in all three sized PM, although high ErFs were occasionally found. This indicates that although such elements mainly originate from geological sources, they sometimes from mixed sources of dust and anthropogenic emissions such as automotive catalyst (Kulkarni et al., 2006). Cerium (Ce), which is one of the lanthanides, had higher ErF values (> 10) in all size-resolved particles than La, Pr, Nd, and Sm, demonstrating that Ce is highly influenced by anthropogenic emissions. For the three size-resolved particles, Ce is highly correlated not only with La, Pr, Nd, and Sm but also with a number of anthropogenic elements, again implying that Ce originated from traffic emissions such as automotive catalyst and fuel additive of diesel vehicles as well as from a crustal source (Kulkarni et al., 2006; Cassee et al., 2011).

High ErFs (> 10) were obtained for As, Ba, Cd, Cu, Cr, Ga, Mo, Sb, Se, and Sn, indicating their anthropogenic origins. Among these elements, Cu is an additive in high temperature lubricant and is present in brake linings, approximately 1–10 % by weight (Sanders et al., 2003), and it has been used successfully as a good tracer for wear emission of road traffic (Pio et al., 2013). Correlation analyses (Table 2) illustrate that Ba, Cd, Ga, Mo, Sb, and Sn are well correlated with Cu ($r > 0.93$) in both coarse and fine modes, suggesting that, similar to Cu, these elements in Hsuehshan Tunnel originated mainly from wear abrasive sources. This could be supported by the presence of both $BaSO_4$ and Sb_2S_3-containing particles in both brake lining materials, in which the former is utilized as a filler and the latter is utilized as an alternative to asbestos (Ingo et al., 2004). Moreover, the use of organic Sb compounds in grease and motor oil is another road traffic emission source of Sb (Huang et al., 1994; Cal-Prieto, 2001).

Lead (Pb) and Zn show high enrichment in all size fractions, indicating that both elements are contributed primarily by traffic emissions, rather than a natural origin. According to the bimodal distribution (Fig. 2) and the good correlations with Cu, Ba, and Sb ($r > 0.67$) in $PM_{1.8–10}$ (Table 2), Zn appears to originate from traffic emissions, and two traffic sources could account for the observed Zn. For the coarse mode, Zn is associated with wear tire debris because Zn is added to tires during vulcanization and is responsible for 1–2 % of the tires by weight (Degaffe and Tuner, 2011; Taheri et al.,

ACPD
14, 13963–14004, 2014

2011). This is in concert with previous results (Adachi and Tainosho, 2004; Councell et al., 2004; Tanner et al., 2008; Harrison et al., 2012). For the fine mode, Zn is probably contributed by lubrication oil via pipe emissions (Huang et al., 1994). Emissions from tailpipe and wear abrasion are both important sources of Pb. However, the size distribution of Pb showed predominance (~ 60 %) in submicron size (Fig. 2). In addition, Pb only correlated moderately with Cu, Sb, and Ba, suggesting that Pb was contributed preferentially by combustion process. A good correlation was observed between Zn and Pb in fine and submicron sizes (Table S2), reflecting tailpipe emissions from vehicles (Wang et al., 2003).

Iron (Fe), which is considered an important crustal element, exhibited enrichment factors of 5 to 11 at the entrance and 12 to 21 at the exit, indicating that Fe in the tunnel was mainly produced from anthropogenic emissions other than road dust. Previous studies have pointed out that in addition to road dust, wear debris from brake linings and tires as well as diesel engine emissions are main sources of Fe in areas near traffic emissions (Cadle et al., 1997; Garg et al., 2000; Wang et al., 2003). In the present study, Fe correlated well with Cu, Ba, and Sb in all sizes ($r > 0.87$, Tables 2 and S2), demonstrating that wear dust is a major anthropogenic source of Fe in Hsuehshan Tunnel, as is the case for those elements.

PCA results are presented in Table 3, in which the data (samples) are divided into three size groups. Two possible sources were identified for coarse PM: wear debris (associated with Fe, Ba, Mn, Cu, Mo, Cd, Sb, and Ga) and road dust (associated with Na, Mg, K, Ca, Ti, and Rb). For fine particles, Fe, Ba, Mn, Cu, Mo, Cd, Sb, Mg, K, Ca, Rb, La, and Ce all had high loadings, whereas Zn and Pb had moderate loadings in PC 1; brake abrasion mixed with re-suspended dust and gasoline emissions might explain this factor. PC 2 in fine mode is related to diesel emissions, as shown by the high positive loading of Zn and the moderate loading of Pb. The third component was identified as road dust because of the correlations among Na, Al, Mg, and K (loadings > 0.4). For submicron particles, high loadings were found for Fe, Ba, Cu, Mo, Sb, Ga and Ce in PC 1. As previously mentioned, Ce in finer PM may be associated with catalyst

ACPD
14, 13963–14004, 2014

converter and fuel additives; therefore, PC 1 might be grouped into mixed sources of wear abrasion and auto catalyst. In addition, good correlations were found for Ca and Mg (loading > 0.6) in submicron particles, which might be produced by diesel engine exhaust (Wang et al., 2003). In PC 2, high positive loadings were found for Pb and Zn, illustrating that exhaust from diesel and gasoline was a potential source in this component. However, PC 3, which had a high loading of Al and a moderate loading of Ca indicates that road dust could be the potential source. PC 4 is a component with high loading for V and Ni. Previous studies have suggested that V and Ni in submicron particles are commonly attributed to fuel oil combustion of diesel engines (Wang et al., 2003; Shafer et al., 2012). As a result, PC 4 was explained by a fuel oil combustion source. Overall, wear abrasion dust and road dust are major sources of many airborne metals over all size ranges inside Hsuehshan Tunnel, and combustion processes from vehicle fleets are additional sources of fine and submicron particles bound metals.

3.4 Fingerprinting ratios of traffic-derived metals

Cu is used as an indicator for wear debris, and the ratios of wear-derived elements to Cu obtained by linear regression approach can be applied to determine the contribution of specific metals from wear debris in urban atmosphere. Figure 4 presents the scatter plots of Fe, Ba, Sb, Sn, Mo, and Ga against Cu in PM_1, $PM_{1-1.8}$, and $PM_{1.8-10}$ at the two sites. These elements had strong correlations ($r > 0.9$), and these ratios were constant in different size-resolved PM, strongly suggesting that these ratios can be applied as good fingerprinting ratios of wear emissions. The mean mass ratios of Fe/Cu, Ba/Cu, Sb/Cu, Sn/Cu, and Ga/Cu were 14, 1.05, 0.16, 0.10 and 0.03, respectively. Table 4 compares our ratios to those established by other tunnel studies. The ratios of Fe/Cu held around 14 to 15 over all sizes in the present work, which agrees with that (14) acquired by dynamometer tests (Sanders et al., 2003) and is also comparable to those observed in different tunnels (Gillies et al., 2001; Fabretti et al., 2009; Cheng et al., 2010b; Pio et al., 2013). However, the Fe/Cu ratio is significantly distinct from those (37 to 60) found in other tunnels; such difference may have arisen

ACPD
14, 13963–14004, 2014

from discrepancies in ingredients of brake pads and in driving conditions (Garg et al., 2000). Ba/Cu ratios of 0.8–1.1 were similar to those found in Europe but slightly lower than that (> 2) found in the United States. Our Sb/Cu ratio of 0.16 is consistent with the result obtained in Hong Kong but lower than that (0.76 to 0.88) occasionally measured in American countries (Gillies et al., 2001; Mancilla and Menodza, 2012). In Japan, Iijima et al. (2007), with the use of dynamometer tests, reported Sb/Cu ratios ranging from 0.05 to 0.11 for different brake pads. They also pointed out that Sb-free brake pads have been utilized recently in Japanese passenger cars. According to the Taiwan Transportation Vehicle Manufactures Association, 44 % and 13 % of vehicle fleets in Taiwan are Japanese and American cars, respectively. The abundance of Japanese cars in Taiwan may have caused the lower Sb/Cu values in this work. For the Mo against Cu scatter plot, two slopes are obtained: 0.05 for coarse and fine particles and 0.12 for particles with aerodynamic diameter less than 0.56 µm. The enhancement of Mo in such submicron particles is perhaps attributed to an additional source of Mo such as diesel exhausts (Kuo et al., 2009). Previous studies show that the ratio of V/Ni has been widely used as a fingerprinting ratio of specific anthropogenic origins. For example, heavy oil combustion shows a narrow range of V/Ni ratio (3 to 4) (Hedberg et al., 2005; Mazzei et al., 2008). Combustion origins from gasoline and diesel vehicles have smaller V/Ni ratios (< 2.0) (Qin et al., 1997; Watson et al., 2001). In this work, V/Ni ratios were typically lower than 2.0 in all size-segregated PM, which were alternatively acquired directly from their mass concentrations (instead of linear regression) because V is not strongly correlated with Ni ($r < 0.5$, Tables 2 and S2) in three different sizes. The lower V/Ni ratios suggest that they were contributed mostly by oil combustion from traffic fleets and partially by heavy oil combustions. The Pb/Cu ratios in the tunnel particles averaged at 0.07, which is much lower than those (much higher than unity) usually observed in ambient air (Fang et al., 2005). In addition, the tunnel particles had As/Sb and Se/Sb ratios of 0.1 and 0.05, respectively, which are also evidently lower than those (around unity) measured in ambient aerosols (Querol et al.,

ACPD
14, 13963–14004, 2014

2007). These results imply that traffic emissions are not major sources of Pb, As, and Se in ambient atmospheres.

Figure 5 illustrates the relationships of La against Ce, Pr, Nd, and Sm. Their correlations weaken with decreasing particle size, suggesting that the REEs in smaller particles were disturbed by certain anthropogenic sources. Ratios of lanthanum to lanthanides have been successfully used to distinguish natural sources from anthropogenic origins (Kulkarni et al., 2006). As shown in Table 5, the La/Ce ratios that range from 0.15 to 0.18 and from 0.10 to 0.12 at the inlet and outlet sites, respectively, are expectedly significantly lower than that of average crust (~ 0.50) (Taylor, 1964) and soils (~ 0.7) (Kulkarni et al., 2006). Such values agree with those of vehicle emissions reported by Kulkarnu et al. (2006) and Huang et al. (1994). As discussed in Sect. 3.3, the ErF values of Ce were mostly higher than unity at both the inlet and outlet sites, with even some of the values being one order of magnitude higher (Fig. 3), revealing that soil dust is not the sole source of Ce. Thus, the low La/Ce values found in the present study could be attributed to an additional supply of Ce from vehicular emissions. In contrast to the La/Ce ratio, the ratios of La/Pr (3.5–7.0), La/Nd (0.5–0.7), and La/Sm (2.1–5.7) were relatively similar to those of soil and crustal materials, as revealed by their resulting ErF of nearly unity, and were very different from those influenced by traffic fleets and petroleum refining (Table 5) (Kulkarni et al., 2006).

3.5 Emission factors of trace elements

As discussed above, 43 % of $PM_{1-1.8}$ and 75 % of $PM_{1.8-10}$ might have been removed during their transport to the outlet site. Therefore, we corrected the EmF that was acquired from the straightforward formulation using Eq. (2) by multiplying the EmF with a factor of 1.43 for $PM_{1.8}$ and 1.75 for $PM_{1.8-10}$.

The resulting EmF of PM_{10} varied from 3.5 to 10.9 mg vkm^{-1}, with an average of 7.7 ± 2.5 mg vkm^{-1}. The EmF of PM_1 averaged at 6.7 mg vkm^{-1}, dominating over PM_{10} emission. Table 6 compiles the data on EmF of varying sized PM that were acquired

ACPD
14, 13963–14004, 2014

during the tunnel experiments. Our EmF was significantly lower than those obtained in other tunnels. Several possible reasons could explain the discrepancy. The length between the two sites inside Hsuehshan Tunnel is one order of magnitude longer than those used in other studies; shorter lengths may not facilitate the dispersion of traffic aerosols, particularly coarser particles. Furthermore, most of the particles would be subject to deposition during advection from the upwind to the downwind sites. This may cause an underestimation of the EmF of super-micron particles, although we have corrected the EmF for fine and coarse particles. Various emission control strategies, including adopting strict standards for new vehicles, scrapping old vehicles, and implementing low-polluted vehicles, have been conducted in the past decade. As shown in Table 6, EmF has exhibited a decreasing trend from the early 1990s to today. The decreasing trends of EmFs for vehicles have also been reported by other studies. Robert et al. (2007) found a significant change in the EmF of $PM_{1.8}$ from 213 mg vkm^{-1} for the old model of LDV (gasoline) to 0.4 mg vkm^{-1} for the new model. In Beijing, emission control strategies have largely reduced $PM_{2.5}$ emission factor of LDV from 8 mg vkm^{-1} in 2010 to an expected 6 mg vkm^{-1} by 2015 (i.e., a reduction rate of 5 % yr^{-1}), leading to a rapid decrease in traffic emissions (Zhang et al., 2014). Accordingly, the lower EmF obtained in Hsuehshan Tunnel might be attributed partly to the success of emission control strategies. Although our EmF was lower than those obtained by other tunnel experiments, it still coincided with those of LDVs (EmF ranged from 2 to 25 mg vkm^{-1} for vehicles manufactured after 1986) by chassis dynamometer tests (Cadle et al., 1999). This suggests that the possibility of overestimating the EmF should be considered carefully when airborne PM measurement is conducted in a tunnel with very short distance.

EmF values of metals were also calculated, as shown in Fig. 6a. On average, the EmFs of all analyzed metals, which represent ~ 4.2 % of PM_{10} mass, were summed to be 327 ± 138 µg vkm^{-1}. The fractions of EmF for each metal in submicron and super-micron particulates are illustrated in Fig. 6b. The wear abrasion related elements, including Cu, Fe, Ba, Cd, Ga, Mo, Mn, Sb, and Sn, were predominant in super-micron

ACPD
14, 13963–14004, 2014

particles. Both Pb and Zn were expectedly dominated by submicron size because their major sources were combustion processes. Geological elements, such as Al, Ca, K, and Mg, were also found mainly in PM_{1-10}. Emissions of REEs, including La, Ce, Pr, Nd, and Sm, were also dominated by super-micron particulates.

Very few studies have addressed traffic emission factor for submicron particles, particularly metallic species (Pant and Harrison, 2013). Meanwhile, the health effects of PM_1 and its accompanying constituents, including carcinogenic metals, are gaining increasing research attention (Donaldson et al., 2002; Schaumann et al., 2004). Thus, we specifically reported the EmFs of traffic-derived metals in PM_1. On average, the EmF of Fe, which is the most abundant element, is $30 \pm 19\ \mu g\ vkm^{-1}$. The EmFs of other traffic-related metals in PM_1 are in the following order: Zn ($9.8\ \mu g\ vkm^{-1}$) > Ba ($1.9\ \mu g\ vkm^{-1}$)> Cu ($1.8\ \mu g\ vkm^{-1}$) > Mn ($1.3\ \mu g\ vkm^{-1}$) > Ti ($0.80\ \mu g\ vkm^{-1}$) > Sb ($0.27\ \mu g\ vkm^{-1}$) > Pb ($0.23\ \mu g\ vkm^{-1}$) > Sn ($0.21\ \mu g\ vkm^{-1}$) > Mo ($0.18\ \mu g\ vkm^{-1}$) > Cr ($0.10\ \mu g\ vkm^{-1}$). Real-world emission factors of wear-related metals have been previously estimated by twin-site studies in Switzerland (Bukowiecki et al., 2009). Our data are highly comparable with their results ($63\ \mu g\ vkm^{-1}$ for Fe, $4.9\ \mu g\ vkm^{-1}$ for Cu, $1.2\ \mu g\ vkm^{-1}$ for Ba, $0.6\ \mu g\ vkm^{-1}$ for Sb, and $0.6\ \mu g\ vkm^{-1}$ for Sn). Although the estimated emission factor may have uncertainties, our data is valuable for future studies on vehicular emission inventory and health effect of PM_1 and its constituents.

Traffic PM emissions are affected by various factors, including driving conditions, vehicle ages, meteorological parameters, and tunnel configurations. Among these parameters, vehicle flows of LDV and HDV (shuttle bus) have been regularly registered by the Taiwan Area National Freeway Bureau (Table 1) to evaluate their affect on EmF. On average, the total numbers of passing vehicles during Sundays were significantly higher ($\sim 20\,\%$) than those on non-Sunday days. This increased traffic flow may alter a few driving conditions and consequently change the traffic emissions of specific elements. For comparison, the EmFs of metals in super-micron particulates (PM_{1-10}) are classified into two groups: Sunday and non-Sunday (Fig. 7). In the Sunday group, the emissions of wear-associated elements were increased by $\sim 50\,\%$ for Ba and up

ACPD
14, 13963–14004, 2014

to ∼ 85 % for Mo. Sternbeck et al. (2002) showed that more wear-related metals (Ba and Sb) are emitted into air by braking when traffic flows increase in tunnels. Likewise, higher emissions of PM_{10}-bearing Cu, Sb, and Ba in Howell Tunnel (Milwaukee, United States) arose from heavy-duty trucks because of their larger tires and amplified brake wear (Lough et al., 2005). Higher traffic flow condition, especially from Sunday late afternoon to Sunday evening when traffic jam is mostly experienced in the tunnel, might render an increased emission of wear metals because a greater number of braking are performed (Li et al., 2011). By contrast, decrease in emissions on Sundays, in comparison with emissions on non-Sundays, was found for various crustal elements, including Al, K, and Rb (by 12 % for K to 53 % for Al). Wind speed and vehicle speed are major factors that control the emissions of re-suspended paved road dust (Ji et al., 1993; Claiborne et al., 1995). They concluded that high wind and vehicle speed are favorable for the resuspension of road dust. In the present work, wind speed did not significantly vary in the tunnel (Table 1), indicating that wind speed is not a major factor affecting the different emissions of crustal metals in our studies. Thus, lower emissions of geological elements on Sunday runs might be attributed to lower traffic speed under higher traffic flow conditions inside Hsuehshan Tunnel (Li et al., 2011), especially for enhanced HDV, at that time.

4 Summary and concluding remarks

Size-fractionated aerosol samples were collected in Hsuehshan Tunnel to characterize particulate metals emitted by vehicle fleets. A total of 36 elements were analyzed by ICP-MS. In terms of their concentrations in PM_{10}, the analyzed elements could be divided into five classes: (1) $\geq 1000\,ng\,m^{-3}$, which includes Fe; (2) 100 to $1000\,ng\,m^{-3}$, which includes Na, Ca, Al, K, Zn, Cu, Ba, and Mg; (3) 10 to $100\,ng\,m^{-3}$, which includes Ti, Mn, Sb; Sn and Cr (4) 1 to $10\,ng\,m^{-3}$, which includes Mo, Pb, Ga, Sr, Ni, V, and Ce; (5) $< 1\,ng\,m^{-3}$, which includes Bi, Hf, Cd, Rb, Se, Nd, Co, As, La, Tl, Y, Sm, Cs, Pr, and U. Compared to the entrance, enhanced concentrations for most metals at the

ACPD
14, 13963–14004, 2014

exit are due to "piston effect". With regard to enrichment factor, correlation matrix, and principal component analysis, the analyzed metals were categorized into three groups, namely, wear abrasion (Cu, Cd, Cu, Fe, Ga, Mn, Mo, Sb, and Sn), re-suspended dust (Ca, Mg, K and Rb), and tailpipe emissions (Zn, Pb and V). Size distributions of these elements were significantly different because of their origins. For wear-related metals and geological elements, a mono-modal size distribution was found and the major peak shifted from the range of 3.2–5.6 µm at the entrance to the range of 1–1.8 µm at the exit. However, elements attributed to combustion sources were predominant mainly in submicron particles and peaked at 0.56–1.0 µm at the inlet site and at 0.18–0.32 µm or 0.32–0.56 µm at the outlet site.

By adopting Cu as an indicator element of wear debris, fingerprinting ratios were constructed, including Fe/Cu, Ba/Cu, Sb/Cu, Sn/Cu and Ga/Cu. These ratios can effectively apportion the source of specific elements in urban environment from wear abrasion. The EmF of all analyzed metals were summed to be 327 ± 138 µg vkm^{-1}, accounting for ~ 4.2 % of PM_{10} emission (7.7 mg vkm^{-1}). Typically, EmFs of given metals attributed to mechanical process such as re-suspended dust and wear emissions were predominant in super-micron mode, whereas combustion origins were mainly in submicron mode. Moreover, different processes that influence the EmFs of wear-related and geological metals were examined in this study.

Although most metal emissions dominated in super-micron PM, the EmFs data of PM_1 metals would be useful for future studies on traffic emission inventory and health effects of submicron PM. Wear abrasion appeared to be a major source of specific toxic elements. While the government focuses on exhaust emission control, the contribution of wear from brake linings and tires might have often been ignored. Thus, stringent implementations of measures for reducing wear emissions are needed in the future.

The Supplement related to this article is available online at doi:10.5194/acpd-14-13963-2014-supplement.

ACPD
14, 13963–14004, 2014

Acknowledgements. This project is part of the "Development of Analytical Tools for Measuring and Characterizing Nanomaterials in the Environment" (EPA-101-1602-02-08 and EPA-102-1602-02-01) and was financially supported by the Environmental Analysis Laboratory of the Environmental Protection Administration in Taiwan. We would like to thank the Directorate General of Highways, MOTC, Taiwan, for supporting the sampling collection in Hsuehshan Tunnel and for providing related information.

References

Abu-Allaban, M., Coulomb, W., Gertler, A. W., Gillies, J., Pierson, W. R., Rogers, C. F., Sagebiel, J. C., and Tarnay, L.: Exhaust particle size distribution measurements at the Tuscarora Mountain Tunnel, Aerosol Sci. Tech., 36, 771–789, doi:10.1080/02786820290038401, 2002.

Adachi, K. and Tainosho, Y.: Characterization of heavy metal particles embedded in the tire dust, Environ. Int., 30, 1009–1017, doi:10.1016/j.envint.2004.04.004, 2004.

Amato, F., Karanasiou, K., Moreno, T., Alastuey, A., Orza, J. A. G., Lumbreras, J., Borge, R., Boldo, E., Linares, C., and Querol, X.: Emission factors from road dust resuspension in a Mediterranean freeway, Atmos. Environ., 61, 580–587, doi:10.1016/j.atmosenv.2012.07.065, 2012.

Birmili, W., Allen, A. G., Bary, F., and Harrison, R. M.: Trace metal concentrations and water solubility in size-fractionated atmospheric particles and influence of road traffic, Environ. Sci. Technol., 40, 1144–1153, doi:10.1021/es0486925, 2006.

Brauer, M. Hoek, G. Vliet, V. P. Meliefste, K., Fischer, P. H., Wijga, A., Koopman, L. P., Neijens, H. J., Gerritsen, J., Kerkhof, M., Heinrich, J., Bellander, T., and Brunekreef, B.: Air pollution from traffic and the development of respiratory infections and asthmatic and allergic symptoms in children, Am. J. Resp. Crit. Care, 166, 1092–1098, doi:10.1164/rccm.200108-007OC, 2002.

Brito, J., Rizzo, L. V., Herckes, P., Vasconcellos, P. C., Caumo, S. E. S., Fornaro, A., Ynoue, R. Y., Artaxo, P., and Andrade, M. F.: Physical–chemical characterisation of the particulate matter inside two road tunnels in the São Paulo Metropolitan Area, Atmos. Chem. Phys., 13, 12199–12213, doi:10.5194/acp-13-12199-2013, 2013.

Bukowiecki, N., Lienemann, P., Hill, M., Figi, R., Richard, A., Furger, M., Rickers, K., Falkenberg, G., Zhao, Y., Cliff, S. S., Prevot, A. S. H., Baltensperger, U., Buchmann, B., and Gehrig, R.:

ACPD
14, 13963–14004, 2014

Rea-world emission factors for antimony and other brak wear related trace elements: size-segregated values for light and heavy duty vehicles, Environ. Sci. Technol., 43, 8072–8078, doi:10.1021/es9006096, 2009.
Cabada, J. C., Rees, S., Takahama, S., Khlystov, A., Pandis, N. S., Davidson, C. I., and Robinson, A. L.: Mass size distributions and size resolved chemical composition of fine particulate matter at the Pittsburg supersite, Atmos. Environ., 38, 3127–3141, doi:10.1016/j.atmosenv.2004.03.004, 2004.
Cadle, S. H., Mulawa, P. A., Ball, J., Donase, C., Weibel, A., Sagebiel, J. C., Knapp, K. T., and Snow, R.: Particulate emission rates from in use high emitting vehicles recruited in Orange County, California, Environ. Sci. Technol., 31, 3405–3412, doi:10.1021/es9700257, 1997.
Cadle, S. H., Mulawa, P. A., Hunsanger, E. C., Nelson, K., Ragazzi, R. A., Barrett, R., Gallagher, G. L., Lawson, D. R., Knapp, K. T., and Snow, R.: Composition of light-duty motor vehicle exhaust particulate matter in the Denver, Colorado area, Environ. Sci. Technol., 33, 2328–2339, doi:10.1021/es9810843, 1999.
Cal-Prieto, M. J., Carlosena, A., Andrade, J. M., Martinez, M. L., Muniategui, S., Lopez-Mahia, P., and Prada, D.: Antinomy as a tracer of the anthropogenic influence on soil and estuarine sediments, Water Air Soil Poll., 129, 333–348, doi:10.1023/A:1010360518054, 2001.
Cassee, F. R., van Balen, E. C., Singh, C., Green, D., Muijser, H., Weinstein, J., and Dreherk, K.: Exposure, health and ecological effects review of engineered nanoscale cerium and cerium oxide associated with its use as a fuel additive, Crit. Rev. Toxicol., 41, 213–229, doi:10.3109/10408444.2010.529105, 2011.
Chang, S.-C., Lin, T.-H., and Lee, C.-T.: On-road emission factors from light-duty vehicles measured in Hsuehshan Tunnel (12.9 km), the longest tunnel in Asia, Environ. Monit. Assess., 153, 187–200, doi:10.1007/s10661-008-0348-9, 2009.
Chen, S.-C., Tsai, C. J., Chou, C. C.-K., Roam, G.-D., Cheng, S.-S., and Wang, Y.-N.: Ultrafine particles at three different sampling locations in Taiwan, Atmos. Environ., 44, 553–540, doi:10.1016/j.atmosenv.2009.10.044, 2010.
Cheng, Y.-H., Liu, Z.-S., and Chen, C.-C.: On-road measurements of ultrafine particle concentration profiles and their size distributions inside the longest highway tunnel in Southeast Asia, Atmos. Environ., 44, 763–772, doi:10.1016/j.atmosenv.2009.11.040, 2010a.
Cheng, Y.-H., Lee, S. C., Ho, K. F., Chow, J. C., Watson, J. G., Louie, P. K. K., Cao, J. J., and Hai, X.: Chemically-speciated on road $PM_{2.5}$ motor vehicle emission factors in Hong Kong, Sci. Total Environ., 408, 1621–1627, doi:10.1016/j.scitotenv.2009.11.061, 2010b.

ACPD
14, 13963–14004, 2014

Chiang, H.-L., and Huang, Y.-S.: Particulate matter emissions from on-road vehicles in a freeway tunnel study, Atmos. Environ., 43, 4014–4022, doi:10.1016/j.atmosenv.2009.05.015, 2009.

Claiborne, C., Mitra, A., Adams, G., Bamesberger, L., Allwine, G., Kantamaneni, R., Lamb, B., and Westerberg, H.: Evaluation of PM_{10} emission rates from paved and unpaved roads using tracer techniques, Atmos. Environ., 29, 1075–1089, doi:10.1016/1352-2310(95)00046-2, 1995.

Councell, T. B., Duckenfield, K. U., Landa, E. R., and Callender, E.: Tire-wear particles as a source of Zn to the environment, Environ. Sci. Technol., 38, 4206–4214, doi:10.1021/es034631f, 2004.

Dall'Osto, M., Querol, X., Amato, F., Karanasiou, A., Lucarelli, F., Nava, S., Calzolai, G., and Chiari, M.: Hourly elemental concentrations in $PM_{2.5}$ aerosols sampled simultaneously at urban background and road site during SAPUSS – diurnal variations and PMF receptor modelling, Atmos. Chem. Phys., 13, 4375–4392, doi:10.5194/acp-13-4375-2013, 2013.

Defino, R. J., Siotuas, C., and Malik, S.: Potential role of ultrafine particles in associations between airborne particle mass and cardiovascular health, Environ. Health Persp., 113, 934–938, doi:10.1289/ehp.7938, 2005.

Degaffe, F. S. and Turner, A.: Leaching of zinc from tire wear particles under simulated estuarine conditions, Chemosphere, 85, 738–743, doi:10.1016/j.chemosphere.2011.06.047, 2011.

Donaldson, K., Tran, C. L., and MacNee, W.: Deposition and effects of fine and ultrafine particles in the respiratory tract, Eur. Respir. Monogr., 21, 77–92, 2002.

Fabretti, J.-F., Sauret, N., Gal, J.-F., Maria, P.-C., and Schärer, U.: Elemental characterization and sources identification of $PM_{2.5}$ using Positive Matrix Factorization: the Malraux road tunnel, Nice, France, Atmos. Res., 94, 320–329, doi:10.1016/j.atmosres.2009.06.010, 2009.

Fang, G.-C., Wu, Y.-S., Huang, S.-H., and Rau, J.-Y.: Review of atmospheric metallic elements in Asia during 2000–2004, Atmos. Environ., 39, 3003–3013, doi:10.1016/j.atmosenv.2005.01.042, 2005.

Funasaka, K., Miyazaki, T., Kawaraya, T., Tsuruho, K., and Mizuno, T.: Characteristics of particulates and gaseous pollutants in a highway tunnel, Environ. Pollut., 102, 171–176, doi:10.1016/S0269-7491(98)00101-8, 1998.

Garg, B. D., Cadle, S. H., Mulawa, P. A., Groblicki, P. J., Laroo, C., and Parr, G. A.: Brake wear particulate matter emissions, Environ. Sci. Technol., 34, 4463–4469, doi:10.1021/es001108h, 2000.

ACPD
14, 13963–14004, 2014

Gillies, J. A., Gertler, A. W., Sagebiel, J. C., and Dippel, W. A.: On-road particulate matter ($PM_{2.5}$ and PM_{10}) emissions in the Sepulveda tunnel, Los Angeles, California, Environ. Sci. Technol., 35, 1054–1063, doi:10.1021/es991320p, 2001.

Grieshop, A. P., Lipsky, E. M., Pekney, N. J., Takahama, S., and Robinson, A. L.: Fine particle emission factors from vehicle in a highway tunnel: effects of fleet composition and season, Atmos. Environ., 40, 287–298, doi:10.1016/j.atmosenv.2006.03.064, 2006.

Handler, M., Puls, C., Zbiral, J., Marr, I., Puxbaum, H., and Limbeck, A.: Size and composition of particulate emissions from motor vehicles in the Kaisermühlen-Tunnel, Atmos. Environ., 42, 2173–2186, doi:10.1016/j.atmosenv.2007.11.054, 2008.

Harrison, R. M., Jones, A. M., Gielt, J., Yin, J., and Green, D. C.: Estimation of the contributions of brake dust, tire wear, and resuspension to nonexhaust traffic particles derived from atmospheric measurements, Environ. Sci. Technol., 46, 6523–6529, doi:10.1021/es300894r, 2012.

He, L. Y., Hu, M., Zhang, Y. H., Huang, X. F., and Yao, T. T.: Fine particle emissions from on-road vehicles in the Zhujiang Tunnel, China, Environ. Sci. Technol., 42, 4461–4466, doi:10.1021/es7022658, 2008.

Hedberg, E., Gidhagen, L., Johansson, C.: Source contributions to PM_{10} and arsenic concentrations in Central Chile using positive matrix factorization, Atmos. Environ., 39, 549–561, doi:10.1016/j.atmosenv.2004.11.001, 2005.

Hee, K. W. and Filip, P.: Performance ceramic enhanced phenolic matrix brake linings materials for automotive brake linings, Wear, 29, 1088–1096, doi:10.1016/j.wear.2005.02.083, 2005.

Hsu, S.-C., Liu, S. C., Huang, Y. T., Lung, S.-C., Tsai, F., Tu, C.-Y., and Kao, S.-J.: A criterion for identifying Asian dust events based on Al concentration data collected from northern Taiwan between 2002 to early 2007, J. Geophys. Res., 113, D18306, doi:10.1029/2007JD009574, 2008.

Hsu, S.-C., Liu, S. C., Huang, Y.-T., Chou, C. C. K., Lung, S. C. C., Liu, T.-H., Tu, J.-Y., and Tsai, F.: Long-range southeastward transport of Asian biosmoke pollution: signature detected by aerosol potassium in Northern Taiwan, J. Geophys. Res., 114, D14301, doi:10.1029/2009JD011725, 2009.

Hsu, S.-C., Liu, S. C., Tsai, F., Engling, G., Lin, I. I., Chou, C. K. C., Kao, S. J., Lung, S. C. C., Chan, C. Y., Lin, S. C., Huang, J. C., Chi, K. H., Chen, W. N., Lin, F. J., Huang, C. H., Kuo, C. L., Wu, T. C., and Huang, Y. T.: High wintertime particulate matter pollution over

ACPD
14, 13963–14004, 2014

a offshore island (Kinmen) off Southeastern China: an overview, J. Geophys. Res., 115, D17309, doi:10.1029/2009JD013641, 2010.
Huang, X., Olmez, I., Aras, N. K., and Gordon, G. E.: Emissions of trace elements from motor vehicles: potential marker elements and source composition profile, Atmos. Environ., 28, 1385–1391, doi:10.1016/1352-2310(94)90201-1, 1994.
Iijima, A., Sato, K., Yano, K., Tago, H., Kato, M., Kimura, H., and Furuta, N.: Particle size and composition distribution analysis of automotive brake abrasion dusts for the evaluation of antimony sources of airborne particulate matter, Atmos. Environ., 41, 4908–4919, doi:10.1016/j.atmosenv.2007.02.005, 2007.
Ingo, G. M., D'Uffizi, M., Falso, G., Bultrini, G., and Padeletti, G.: Thermal and microchemical investigation of automotive brake pad wear residues, Thermochim. Acta, 418, 61–68, doi:10.1016/j.tca.2003.11.042, 2004.
Ji, X., Jiang, D., Fei, S., Fe, Yuan, H., He, P., Ye, B., Lei, Z., and Feng, C.: Road dust emission inventory for the metropolitan area of Shanghai City, Atmos. Environ., 27, 1736–1741, doi:10.1016/0960-1686(93)90237-S, 1993.
Johansson, C., Norman, M., and Burman, L.: Road traffic emission factors for heavy metals, Atmos. Environ., 43, 4681–4688, doi:10.1016/j.atmosenv.2008.10.024, 2009.
Kulkarni, P., Chellam, S., and Fraser, M. P.: Lanthanum and lanthanides in atmospheric fine particles and their apportionment to refinery and petrochemical operations in Houston, TX, Atmos. Environ., 40, 508–520, doi:10.1016/j.atmosenv.2005.09.063, 2006.
Kuo, C.-Y., Wang, J.-Y., Chang, S.-H., and Chen, M.-C.: Study of metal concentrations in the environment near diesel transport routes, Atmos. Environ., 43, 3070–3076, doi:10.1016/j.atmosenv.2009.03.028, 2009.
Lai, C.-H., and Peng, Y.-P.: Volatile hydrocarbon emissions from vehicles and vertical ventilations in the Hsuehshan traffic tunnel, Taiwan, Environ. Monit. Assess., 184, 4015–4028, doi:10.1007/s10661-011-2240-2, 2012.
Lawrence, S., Sokhi, R., Ravindra, K, Mao, H., Prain, H. D., and Bull, I. D.: Source apportionment of traffic emissions o particulate matter using tunnel measurements, Atmos. Environ., 77, 548–557, doi:10.1016/j.atmosenv.2013.03.040, 2013
Li, H.-C., Chen, K. S., Lai, C.-H., and Wang, H.-K.: Measurements of gaseous pollutant concentrations in the Hsuehshan traffic tunnel of Northern Taiwan, Aerosol Air Qual. Res., 11, 776–782, doi:10.4209/aaqr.2011.02.0009, 2011.

ACPD
14, 13963–14004, 2014

Lin, C.-C., Chen, S.-J., Huang, K.-L., Hwang, W.-I., Chang-Chien, G. P., and Lin, W. Y.: Characteristics of metals in nano/ultrafine/fine/coarse particles collected beside a heavily trafficked road, Environ. Sci. Technol., 39, 8113–8125, doi:10.1021/es048182a, 2005.

Lough, G. C., Schauer, J. J., Park, J.-S., Shafer, M. M., Deminter, J. T., and Weinstein, J. P.: Emissions of metal associated with motor vehicle roadways, Environ. Sci. Technol., 39, 826–836, doi:10.1021/es048715f, 2005.

Mancilla, Y. and Mendoza, A.: A tunnel study to characterize $PM_{2.5}$ emissions from gasoline-powered vehicles in Monterrey, Mexico, Atmos. Environ., 59, 449–460, doi:10.1016/j.atmosenv.2012.05.025, 2012.

Mazzei, F., D'Alessandro, A., Lucarelli, F., Nava, S., Prati, P., Valli, G., and Vecchi, R.: Characterization of particulate matter sources in an urban environment, Sci. Total Environ., 401, 81–89, doi:10.1016/j.scitotenv.2008.03.008, 2008.

Moreno, T., Pérez, N., Reche, C., Martins, C., de Miguel, E., Capdevila, M., Centelles, S., Minguillón, M. C., Amato, F., Alastuey, A., Querol, X., and Gibbson, W.: Subway platform air quality: assessing the influences of tunnel ventilation, train piston effect and station design, Atmos. Environ., 92, 461–468, doi:10.1016/j.atmosenv.2014.04.043, 2014.

Nel, A.: Air pollution-related illness: effects of particle, Science, 308, 804–806, doi:10.1126/science.1108752, 2005.

Pant, P. and Harrison, R. M.: Estimation of the contribution of road traffic emissions to particulate matter concentrations from field measurements: a review, Atmos. Environ., 77, 78–97, doi:10.1016/j.atmosenv.2013.04.028, 2013.

Pierson, W. R., Gertler, A. W., Robinson, N. F., Sagebiel, J. C., Zielinska, B., Bishop, G. A., Stedman, D. H., Zweidinger, R. B., and Ray, W.: Real-world automotive emissions-summary of studies in the Fort McHenry and Tuscarora Mountain Tunnels, Atmos. Environ., 30, 2233–2256, doi:10.1016/1352-2310(95)00276-6, 1996.

Pio, C., Mirante, F., Oliveira, C., Matos, M., Caseiro, A., Oliveira, C., Querol, X., Alves, C., Martins, N., Cerqueira, M., Camões, F., Silva, H., and Plana, F.: Size-segregated chemical composition of aerosol emissions in an urban road tunnel in Portugal, Atmos. Environ., 71, 15–25, doi:10.1016/j.atmosenv.2013.01.037, 2013.

Qin, Y., Chan, K. C., and Chan, Y. L.: Characteristics of chemical compositions of atmospheric aerosol in Hong Kong, spatial and seasonal distributions, Sci. Total Environ., 206, 25–37, doi:10.1016/S0048-9697(97)00214-3, 1997.

ACPD
14, 13963–14004, 2014

Querol, X., Viana, M., Alastuey, A., Amato, F., Moreno, T., Castillo, S., Pey, J., de la Rosa, J., Sánchez de la Campa, A., Artíñano, B., Salvador, P., García Dos Santos, S., Fernández-Patier, R., Moreno-Grau, S., Negral, L., Minguillón, M. C., Monfort, E., Gil, J. I., Inza, A., Ortega, L. A., Santamaría, J. M., and Zabalza, J.: Source origin of trace elements in PM from regional background, urban and industrial sites of Spain, Atmos. Environ., 41, 7219–7231, doi:10.1016/j.atmosenv.2007.05.022, 2007.

Robert, M. A., Vanbergen, S., Kleeman, M. J., and Jakober, C. A.: Size and composition distributions of particulate matter emissions: part 1 – light duty gasoline vehicles, JAPCA J. Air Waste Ma., 57, 1414–1428, doi:10.3155/1047-3289.57.12.1414, 2007.

Rogge, W. F., Hildemann, L. M., Mazurek, M. A., Cass, G. R., and Simoneit, B. R. T.: Sources of fine organic aerosol. 3. Road dust, tire debris, and organometallic brake lining dust-roads as source and sinks, Environ. Sci. Technol., 27, 1892–1904, doi:10.1021/es00046a019, 1993.

Sanders, P. G., Xu, N., Dalka, T. M., and Maricq, M. M.: Airborne brake wear debris: size distributions, composition, and a comparison of dynamometer and vehicle tests, Environ. Sci. Technol., 37, 4060–4069, doi:10.1021/es034145s, 2003.

Schaumann, F., Borm, P. J. A., Herbrich, A., Knoch, J., Pitz, M., Roel, P. F., Schins, Luettig, B., Hohlfeld, J. M., Heinrich, J., and Krug, N.: Metal-rich ambient particles (particulate matter 2.5) cause airway inflammation in healthy subjects, Am. J. Resp. Crit. Care, 170, 898–903, doi:10.1164/rccm.200403-423OC, 2004.

Shafer, M. M., Toner, B. M., Overdier, J. T., Schauer, J. J., Fakra, S. C., Hu, S., Herner, J. D., and Ayala, A.: Chemical speciation of vanadium in particulate matter emitted from diesel vehicles and urban atmospheric aerosols, Environ. Sci. Technol., 46, 189–195, doi:10.1021/es200463c, 2012.

Sternbeck, J., Sjödin, Å., and Andréasson, K.: Metal emissions from road traffic and the influence of resuspension-results from two tunnel studies, Atmos. Environ., 36, 4735–4744, doi:10.1016/S1352-2310(02)00561-7, 2002.

Taheri, S., Khoshgoftarmanesh, A. H., Shariatmadari, H., and Chaney, R. L.: Kinetics of zinc release from ground tire rubber and rubber ash in a calcareous soil as alternatives to Zn fertilizers, Plant Soil, 341, 89–91, doi:10.1007/s11104-010-0624-7, 2011.

Thorp, A. and Harrison, R. M.: Sources and properties of non-exhaust particulate matter from road traffic: a review, Sci. Total Environ., 400, 270–282, doi:10.1016/j.scitotenv.2008.06.007, 2008.

ACPD
14, 13963–14004, 2014

Tanner, P. A., Hoi-Ling, M., and Yu, P. K. N.: Fingerpriting metals in urban street dust in Beijing, Shanghai and Hong Kong, Environ. Sci. Technol., 42, 7111–7117, doi:10.1021/es8007613, 2008.

Taylor, S. R.: Abundance of chemical elements in the continental crust: a new table, Geochim. Cosmochim. Ac., 18, 1273–1285, doi:10.1016/0016-7037(64)90129-2, 1964.

Wåhlin, P., Berkowicz, R., and Palmgren, F.: Characterization of traffic-generated particulate matter in Copenhagen, Atmos. Environ., 40, 2151–2159, doi:10.1016/j.atmosenv.2005.11.049, 2006.

Wang, Y.-F., Huang, K.-L., Li, C.-T., Mi. H.-H., Luo, J.-H., and Tsai, P.-J.: Emissions of fuel metals content from a diesel vehicle engine, Atmos. Environ., 33, 4637–4643, doi:10.1016/j.atmosenv.2003.07.007, 2003.

Watson, J., Chow, J., and Houck, J. E.: $PM_{2.5}$ chemical source profiles for vehicle exhaust, vegetative burning, geological material and coal burning in Northwestern Colorado during 1995, Chemosphere, 43, 1141–1151, doi:10.1016/S0045-6535(00)00171-5, 2001.

Weingartner, E., Keller, C., Stahel, W. A., Burtscher, H., and Baltensperger, U.: Aerosol emission in a road tunnel, Atmos. Environ., 31, 451–462, doi:10.1016/S1352-2310(96)00193-8, 1997.

Zhang, R., Jing, J., Tao, J., Hsu, S.-C., Wang, G., Cao, J., Lee, C. S. L., Zhu, L., Chen, Z., Zhao, Y., and Shen, Z.: Chemical characterization and source apportionment of $PM_{2.5}$ in Beijing: seasonal perspective, Atmos. Chem. Phys., 13, 7053–7074, doi:10.5194/acp-13-7053-2013, 2013.

Zhang, S., Wu, Y., Wu, X., Li, M., Ge, Y., Liang, B., Xu, Y., Zhou, Y., Liu, H., Fu, L., and Hao, J., Historic and future trends of vehicle emissions in Beijing, 1998–2020: a policy assessment for the most stringent vehicle emission control program in China, Atmos. Environ., 89, 216–229, doi:10.1016/j.atmosenv.2013.12.002, 2014.

Zhu, C.-S., Chen, C.-C., Cao, J.-J., Tsai, C.-J., Chou, C.-K., Liu, S.-C., and Roam, G.-D.: Characterization of carbon fractions for atmospheric fine particles and nonoparticles in a highway tunnel, Atmos. Environ., 44, 2668–2673, doi:10.1016/j.atmosenv.2010.04.042, 2010.

ACPD
14, 13963–14004, 2014

Table 1. Summary of sampling dates, mass concentrations ($\mu g\,m^{-3}$) of $PM_{1.8-10}$, $PM_{1-1.8}$ and PM_1 as well as traffic flow and wind speed in Hsuehshan Tunnel during the sampling periods in 2013.

Sampling No.	Date	Inlet Site			Outlet Site			Vehicle fleet		Wind Speed
		$PM_{1.8-10}$	$PM_{1-1.8}$ ($\mu g\,m^{-3}$)	PM_1	$PM_{1.8-10}$	$PM_{1-1.8}$ ($\mu g\,m^{-3}$)	PM_1	LDV (No. h^{-1})	HDV (No. h^{-1})	($m\,s^{-1}$)
1	17 May 2013	17	4	32	17	9	155	1272	72	4.7
2	18 May 2013	18	7	43	18	11	128	1777	88	4.6
3	19 May 2013	19	6	35	21	12	208	1843	109	4.7
4	19 Jul 2013	16	4	27	26	9	83	1277	104	4.3
5	20 Jul 2013	16	3	34	15	9	142	1400	118	4.8
6	21 Jul 2013	13	3	33	20	9	168	1680	126	4.7
7	8 Aug 2013	17	4	26	15	11	142	1354	109	4.7
8	9 Aug 2013	19	4	39	9	10	87	1460	133	5.2
9	10 Aug 2013	9	3	23	16	10	126	1712	81	4.9
10	27 Sep 2013	27	4	22	28	10	125	1334	81	4.7
11	28 Sep 2013	22	4	39	16	9	85	1764	101	5.0
12	29 Sep 2013	15	4	34	18	10	180	1909	121	4.7

ACPD
14, 13963–14004, 2014

Table 2. Correlation matrix of selected elements in coarse (top side triangle) and fine particles (lower side triangle) observed in Hsuehshan Tunnel. Correlation coefficients higher than 0.8 are marked in bold.

	Al	Fe	Mg	K	Ca	Sr	Ba	Ti	Mn	Ni	Cu	Zn	Mo	Cd	Sn	Sb	Pb	V	Cr	Rb	Cs	Ga	La	Ce	Pr	Nd
Al		0.29	0.42	0.44	0.44	0.45	0.29	0.35	0.34	0.05	0.25	0.43	0.16	0.19	0.17	0.17	0.49	0.20	0.10	0.47	0.41	0.30	0.40	0.20	0.45	0.25
Fe	0.69		0.27	0.31	0.43	**0.88**	**0.97**	**0.96**	**1.00**	−0.03	**0.99**	0.66	**0.98**	**0.97**	**0.97**	**0.98**	0.64	0.74	0.57	0.41	0.38	**0.96**	0.71	**0.91**	0.73	**0.90**
Mg	0.78	**0.84**		0.74	0.61	0.62	0.36	0.44	0.30	−0.09	0.24	0.31	0.23	0.29	0.29	0.24	0.62	0.42	0.03	0.75	0.62	0.38	0.66	0.44	0.55	0.50
K	0.71	**0.89**	**0.84**		0.61	0.63	0.45	0.44	0.36	0.25	0.22	0.56	0.25	0.32	0.31	0.26	0.68	0.45	0.37	0.91	**0.88**	0.45	0.68	0.48	0.69	0.55
Ca	0.70	**0.86**	**0.82**	**0.86**		0.75	0.57	0.56	0.48	−0.05	0.38	0.59	0.39	0.48	0.47	0.46	**0.90**	0.49	0.13	**0.81**	0.74	0.61	**0.82**	0.47	0.74	0.55
Sr	0.64	**0.99**	**0.86**	**0.89**	**0.88**		**0.94**	**0.93**	**0.90**	−0.04	**0.83**	0.76	**0.83**	**0.88**	**0.87**	**0.86**	**0.87**	0.75	0.45	0.75	0.67	**0.94**	**0.90**	**0.86**	**0.88**	**0.90**
Ba	0.60	**0.98**	**0.81**	**0.87**	**0.82**	**0.99**		**0.95**	**0.97**	−0.04	**0.93**	0.77	**0.94**	**0.96**	**0.96**	**0.96**	0.75	0.73	0.52	0.56	0.52	**1.00**	**0.81**	**0.91**	**0.82**	**0.92**
Ti	0.68	**0.99**	**0.85**	**0.87**	**0.84**	**0.98**	**0.97**		**0.96**	0.02	**0.96**	0.70	**0.95**	**0.96**	**0.96**	**0.96**	0.75	0.79	0.50	0.55	0.51	**0.95**	**0.80**	**0.88**	0.75	**0.89**
Mn	0.63	**0.95**	**0.80**	**0.90**	**0.91**	**0.95**	**0.95**	**0.93**		0.45	**0.98**	0.69	**0.97**	**0.96**	**0.97**	**0.97**	0.68	0.75	0.60	0.46	0.43	**0.97**	0.74	**0.90**	0.76	**0.90**
Ni	0.01	0.08	0.02	0.11	−0.01	0.05	0.06	0.06	0.12		−0.09	−0.02	−0.07	−0.11	−0.10	−0.09	−0.03	−0.02	0.73	0.15	0.16	−0.05	0.05	0.00	0.06	0.03
Cu	0.66	**0.99**	**0.83**	**0.85**	**0.82**	**0.98**	**0.97**	**1.00**	**0.93**	0.06		0.63	**0.99**	**0.97**	**0.98**	**0.98**	0.60	0.73	0.51	0.32	0.30	**0.93**	0.66	**0.87**	0.64	**0.85**
Zn	0.22	0.50	0.34	0.55	0.61	0.50	0.52	0.47	0.72	0.43	0.45		0.63	0.72	0.67	0.67	0.76	0.49	0.31	0.56	0.51	0.78	0.67	0.56	0.65	0.60
Mo	0.61	**0.98**	**0.81**	**0.84**	**0.82**	**0.98**	**0.98**	**0.99**	**0.93**	0.05	**0.99**	0.47		**0.98**	**0.99**	**0.99**	0.60	0.75	0.54	0.34	0.33	**0.93**	0.67	**0.88**	0.65	**0.86**
Cd	0.56	**0.96**	0.76	**0.86**	**0.87**	**0.95**	**0.96**	**0.95**	**0.98**	0.17	**0.95**	0.70	**0.96**		**1.00**	**0.99**	0.68	0.73	0.49	0.43	0.41	**0.96**	0.72	**0.87**	0.69	**0.86**
Sn	0.60	**0.98**	**0.80**	**0.84**	**0.83**	**0.98**	**0.97**	**0.99**	**0.93**	0.05	**0.99**	0.48	**1.00**	**0.96**		**0.99**	0.66	0.74	0.51	0.41	0.40	**0.95**	0.72	**0.89**	0.69	**0.88**
Sb	0.63	**0.99**	**0.81**	**0.85**	**0.85**	**0.98**	**0.98**	**0.99**	**0.94**	0.05	**0.99**	0.50	**0.99**	**0.97**	**1.00**		0.64	0.74	0.52	0.38	0.36	**0.95**	0.71	**0.87**	0.68	**0.86**
Pb	0.59	0.73	0.76	**0.84**	**0.89**	0.75	0.70	0.71	**0.85**	0.21	0.69	0.75	0.68	**0.80**	0.70	0.70		0.62	0.27	**0.81**	0.73	0.77	**0.91**	0.64	0.78	0.70
V	0.28	0.39	0.31	0.49	0.35	0.38	0.38	0.41	0.37	0.22	0.40	0.20	0.42	0.40	0.39	0.38	0.44		0.45	0.54	0.52	0.73	0.71	0.72	0.65	0.75
Cr	0.20	0.41	0.28	0.30	0.27	0.38	0.39	0.38	0.44	**0.84**	0.39	0.60	0.38	0.49	0.39	0.38	0.40	0.11		0.31	0.32	0.49	0.37	0.53	0.44	0.54
Rb	0.64	**0.81**	0.74	**0.92**	**0.92**	**0.83**	0.79	0.78	**0.89**	0.07	0.75	0.64	0.75	**0.82**	0.76	0.77	**0.90**	0.40	0.27		**0.96**	0.56	**0.82**	0.57	**0.83**	0.65
Cs	0.50	0.65	0.56	**0.80**	**0.82**	0.67	0.64	0.61	0.77	0.11	0.58	0.65	0.58	0.70	0.60	0.61	**0.84**	0.44	0.23	**0.95**		0.51	0.74	0.53	0.77	0.61
Ga	0.60	**0.99**	**0.81**	**0.85**	**0.85**	**0.99**	**0.99**	**0.98**	**0.95**	0.06	**0.98**	0.53	**0.98**	**0.97**	**0.99**	**0.98**	0.71	0.38	0.40	0.79	0.63		**0.82**	**0.90**	**0.82**	**0.91**
La	0.71	**0.87**	**0.81**	**0.88**	**0.94**	**0.88**	**0.82**	**0.85**	**0.88**	0.04	**0.83**	0.52	**0.83**	**0.84**	**0.84**	**0.84**	**0.87**	0.44	0.32	**0.89**	0.77	**0.84**		0.79	**0.89**	**0.84**
Ce	0.60	**0.89**	**0.80**	**0.81**	0.78	**0.90**	**0.86**	**0.88**	**0.81**	0.00	**0.89**	0.30	**0.90**	**0.81**	**0.89**	**0.87**	0.67	0.36	0.32	0.72	0.54	**0.87**	**0.87**		**0.83**	**0.99**
Pr	0.68	**0.90**	**0.81**	**0.89**	**0.82**	**0.92**	**0.89**	**0.87**	**0.87**	0.01	**0.86**	0.43	**0.86**	**0.82**	**0.85**	**0.85**	0.70	0.28	0.31	**0.85**	0.68	**0.87**	**0.85**	**0.87**		**0.88**
Nd	0.62	**0.91**	**0.82**	**0.83**	**0.82**	**0.92**	**0.88**	**0.91**	**0.84**	0.01	**0.91**	0.32	**0.92**	**0.84**	**0.91**	**0.89**	0.70	0.36	0.32	0.76	0.57	**0.89**	**0.90**	**1.00**	**0.90**	

ACPD
14, 13963–14004, 2014

Table 3. Summaries of principal component analysis for trace metals in coarse, fine and submicron particles observed in Hsuehshan Tunnel. Factor loadings lower than ±0.4 are not given. Loading factor greater than 0.7 is marked by bold.

	Coarse		Fine			Submicron			
	PC1	PC2	PC1	PC2	PC3	PC1	PC2	PC3	PC4
Al		0.55	0.52		0.68			**0.88**	
Fe	**0.98**		**0.94**			**0.82**	0.52		
Na		**0.81**			**0.93**				
Mg		**0.89**	**0.70**		0.66	0.69			
K		**0.88**	**0.77**		0.44		0.57		
Ca		**0.75**	**0.81**			0.65		0.53	
Ba	**0.94**		**0.95**			**0.96**			
Ti	**0.93**		**0.94**			**0.73**			
Mn	**0.97**		**0.90**				**0.96**		
Ni				**0.76**				0.56	**0.72**
Cu	**0.98**		**0.95**			**0.96**			
Zn	0.65	0.42	0.44	**0.79**			**0.97**		
Mo	**0.99**		**0.96**			**0.96**			
Cd	**0.97**		**0.92**				**0.90**		
Sb	**0.99**		**0.96**			**0.90**			
Pb	0.58	**0.71**	0.62	0.61			**0.84**		
V	**0.72**								**0.92**
Rb		**0.90**	**0.73**	0.44			0.63		
Ga	**0.93**		**0.96**			**0.94**			
La	0.65	0.68	**0.80**			**0.81**			
Ce	**0.86**		**0.86**			**0.92**			
Potential source	Wear debris	Dust	Wear debris + Dust + Gasoline	Tailpipe emission	Dust	Wear debris + Auto catalyst	Tailpipe emission	Dust	Fuel oil

ACPD
14, 13963–14004, 2014

Table 4. Ratios of specific elements to Cu in tunnel PM.

Tunnel studies	Size	Fe/Cu	Ba/Cu	Sb/Cu	Sn/Cu	Reference[b]
Hatfield Tunnel (UK)	PM_{10}	19	1.23	0.13		1
Marquês de Pombal Tunnel (Portugal)	$PM_{0.5-10}$	16	0.27	0.08	0.23	2
Tsngstad Tunnel (Sweden)	PM_{10}	28	0.74	0.18		3
Lundby Tunnel (Sweden)	PM_{10}	60	1.34	0.24		3
Malraux Tunnel (France)	$PM_{2.5}$	15		0.14	0.14	4
Squirrel Hill Tunnel (USA)[a]	$PM_{2.5}$	37	2.48	0.21	0.48	5
Sepulveda Tunnel (USA)[a]	$PM_{2.5}$	16	2.12	0.88	0.82	6
Loma Largo Tunnel (Mexico)	$PM_{2.5}$	7	0.13	0.76	0.49	7
Jānio Tunnel (Brazil)	$PM_{2.5}$	20		0.12		8
Belway Rodonael Mário Covas Tunnel (Brazil)	$PM_{2.5}$	45		0.36		8
Shing Mun Tunnel (Hong Kong)	$PM_{2.5}$	17	0.58	0.14	0.29	9
Zhuijiang Tunnel (China)	$PM_{2.5}$	28	1.08			10
Hsuehshan Tunnel (Taiwan)	$PM_{1.8-10}$	14	0.80	0.14	0.09	
	$PM_{1-1.8}$	14	1.07	0.16	0.09	This study
	PM_1	15	1.10	0.16	0.11	

[a] The ratios of Squirrel Hill Tunnel and Sepulveda Tunnel are obtained from the ratios of elemental emission factors.

[b] 1: Lawrence et al. (2013); 2: Pio et al. (2013); 3: Sternbeck et al. (2002); 4: Fabretti et al. (2009); 5: Grieshop et al. (2006); 6: Gillies et al. (2001); 7: Mancilla and Mendoza (2012); 8: Brito et al. (2013); 9: Cheng et al. (2010b); 10: He et al. (2008).

ACPD
14, 13963–14004, 2014

Table 5. Ratios of La to lanthanides in ariborne PM collected in Hsuehshan Tunnel, and comparison to other emission sources reported in the literature.

	Size	This study[a]	Soil[b]	Crustal materials[c]	Auto catalyst[b]	Petrolium refining[b]	Washburn tunnel[b]	Motor catalyst[d]
La/Ce	$PM_{1.8-10}$	0.18 (0.12)	0.7	0.5	0.7	4.3	0.2	0.13
	$PM_{1-1.8}$	0.18 (0.11)						
	PM_1	0.15 (0.12)						
La/Pr	$PM_{1.8-10}$	7.00 (5.08)	0.7	3.7	9.4	9.7	95.6	
	$PM_{1-1.8}$	6.53 (4.74)						
	PM_1	6.78 (3.46)						
La/Nd	$PM_{1.8-10}$	0.68 (0.47)	2.1	1.1	2.9	6.4	36.3	
	$PM_{1-1.8}$	0.69 (0.47)						
	PM_1	0.71 (0.48)						
La/Sm	$PM_{1.8-10}$	3.86 (3.59)	3.9	5.0	200.7	55.2		0.004
	$PM_{1-1.8}$	3.61 (2.13)						
	PM_1	4.76 (5.69)						

[a] Values in the parenthases are the ratios obtained at the outlet site.
[b] Kulkarni et al. (2006).
[c] Taylor et al. (1964).
[d] Huang et al. (1994).

ACPD
14, 13963–14004, 2014

Table 6. Comparison of emission factors of PM mass in this work and other tunnel studies.

Tunnel studies	Studied Year	Length[a] (km)	Traffic Flow (vehicles h^{-1})	Size	Emission Factor (mg vkm^{-1})	Reference[b]
Kaisermühlen Tunnel(Austra)	2005	2.1	200–500 (> 4 % of HDV)	PM_{10}	62	1
				$PM_{2.5}$	26	1
Gubrist Tunnel (Swizerland)	1993	3.1		PM_3	310	2
Squirrel Hill Tunnel (USA)	2002	1.3	2303 (8 % of HDV)	$PM_{2.5}$	189	3
Sepulveda Tunnel (USA)	1996	0.6	3037 (3 % of HDV)	$PM_{2.5}$	52	4
Tsngstad Tunnel (Sweden)	1999	0.5	2978 (10 % of HDV)	PM_{10}	44	5
Lundby Tunnel (Sweden)	2000	2.0	1407 (14 % of HDV)	PM_{10}	285	5
Loma Largo Tunnel (Mexico)	2009	0.2		$PM_{2.5}$	23	6
Shing Mun Tunnel (Hong Kong)	2003	3.0	1600	$PM_{2.5}$	131	7
Chung-Liao Tunnel (Taiwan)	2005	1.1	720–2050 (12 % of HDV)	$PM_{2.5-10}$	18	8
				$PM_{2.5}$	38	8
Hsuehshan Tunnel (Taiwan)	2013	8.9	1669 (6 % in HDV)	PM_1	7	This study

[a] Length is the distance between inlet and outlet sampling sites.
[b] 1: Handler et al. (2008); 2: Weingartner et al. (1997); 3: Grieshop et al. (2006); 4: Gillies et al. (2001); 5: Sternbeck et al. (2002); 6: Mancilla and Mendoza (2012); 7: Cheng et al. (2010); 8: Chiang and Huang (2009).

ACPD
14, 13963–14004, 2014

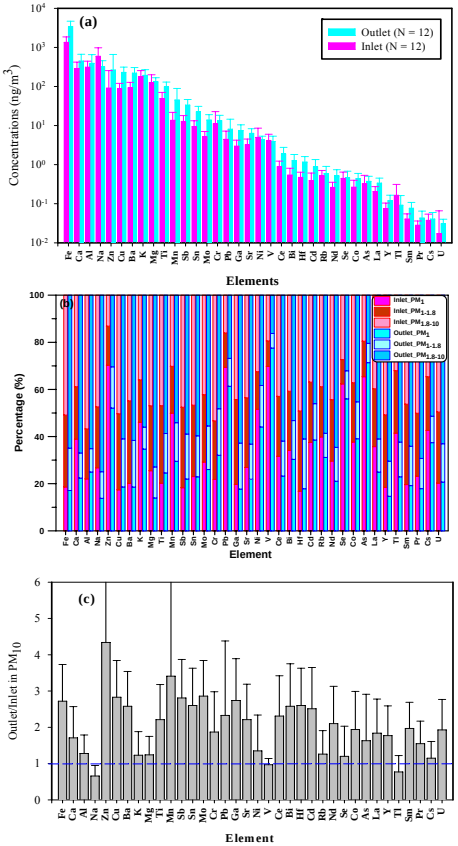

Figure 1. (a) Elemental compositions of PM_{10} collected at both the inlet and outlet sites in Hsuehshan Tunnel; **(b)** partitioning of trace metals within three sized PM; **(c)** outlet-to-inlet ratio for each element in PM_{10}. The sequence of metallic species is in order of decreasing concentrations (ng m^{-3}) at the outlet site. *N* denotes the number of aerosol samples.

ACPD
14, 13963–14004, 2014

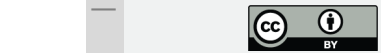

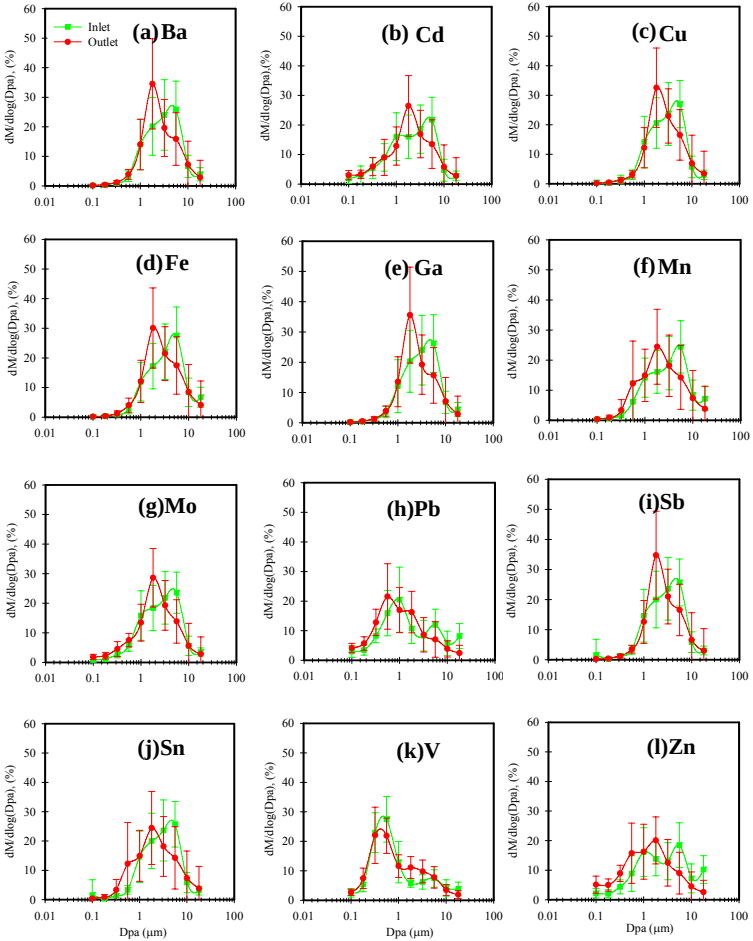

Figure 2. Average size distributions of traffic-derived elements observed at the inlet and outlet sites inside Hsuehshan Tunnel.

ACPD
14, 13963–14004, 2014

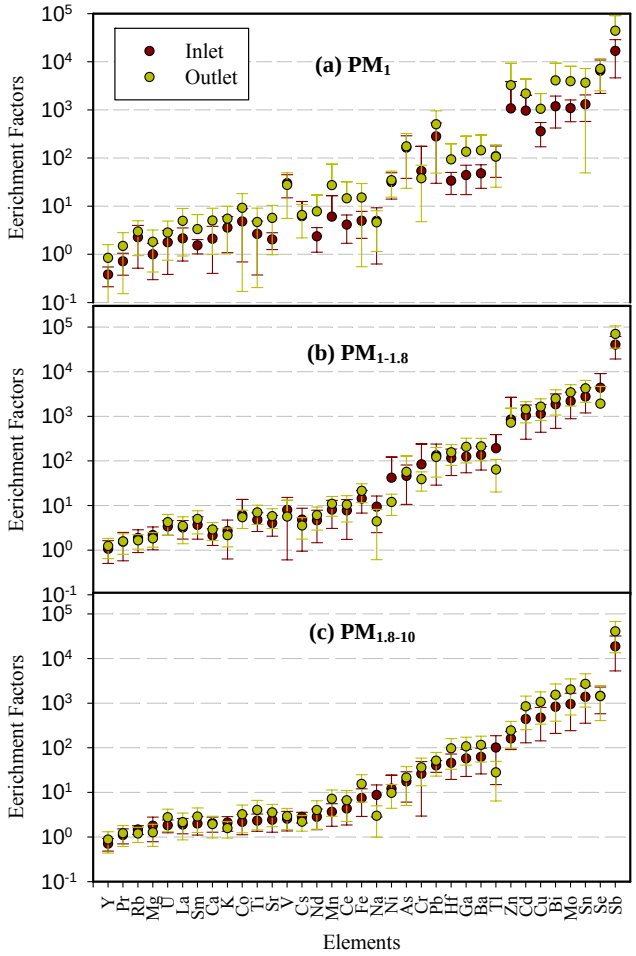

Figure 3. Enrichment factors of trace metals in **(a)** PM_1, **(b)** $PM_{1–1.8}$ and **(c)** $PM_{1.8–10}$ observed at the inlet and outlet sites in Hsuehshan Tunnel.

ACPD
14, 13963–14004, 2014

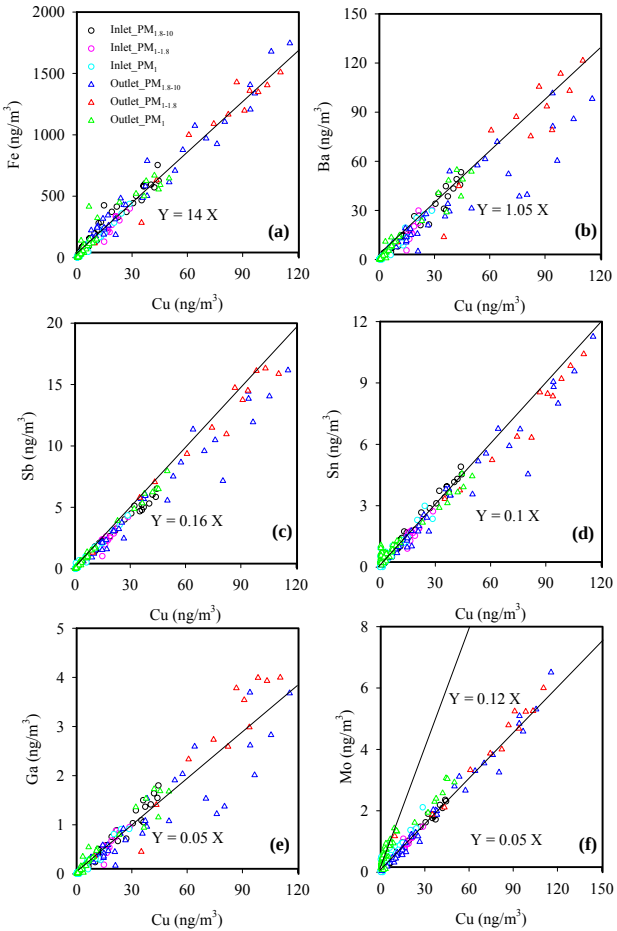

Figure 4. Scatter plots of **(a)** Fe, **(b)** Ba, **(c)** Sb, **(d)** Sn, **(e)** Ga, **(f)** Mo against Cu concentrations (ng m^{-3}) in different size-segregated particles observed in Hsuehshan Tunnel.

ACPD
14, 13963–14004, 2014

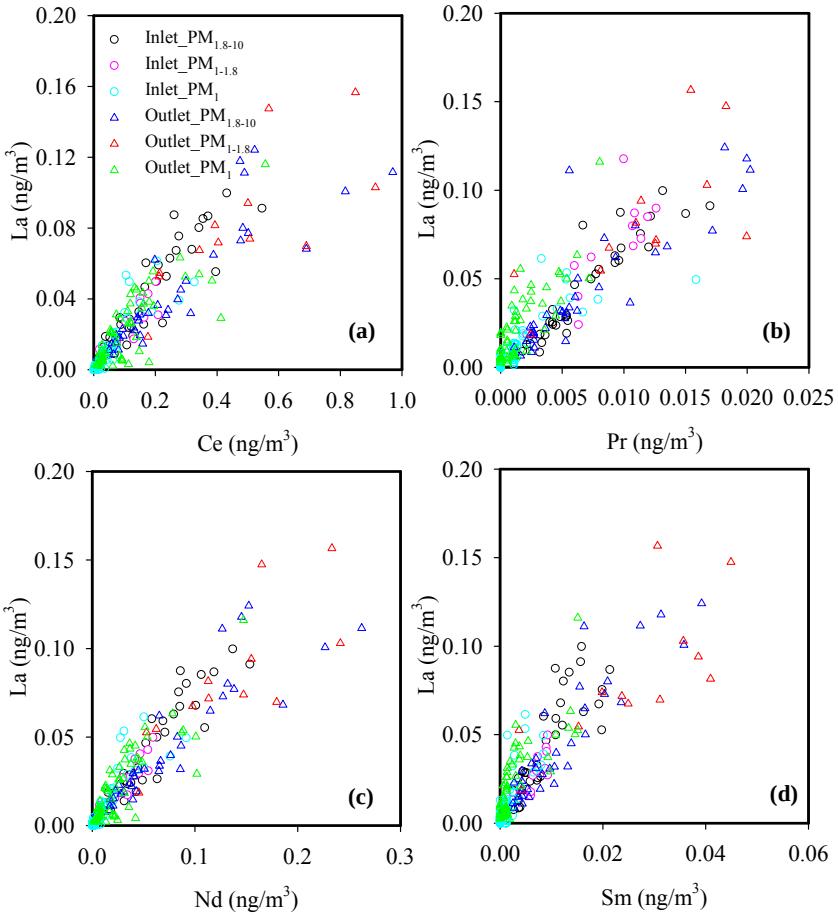

Figure 5. Scatter plots of La and **(a)** Ce, **(b)** Pr, **(c)** Nd and **(d)** Sm concentrations (ng m^{-3}) in different size-segregated particles observed in Hsuehshan Tunnel

ACPD
14, 13963–14004, 2014

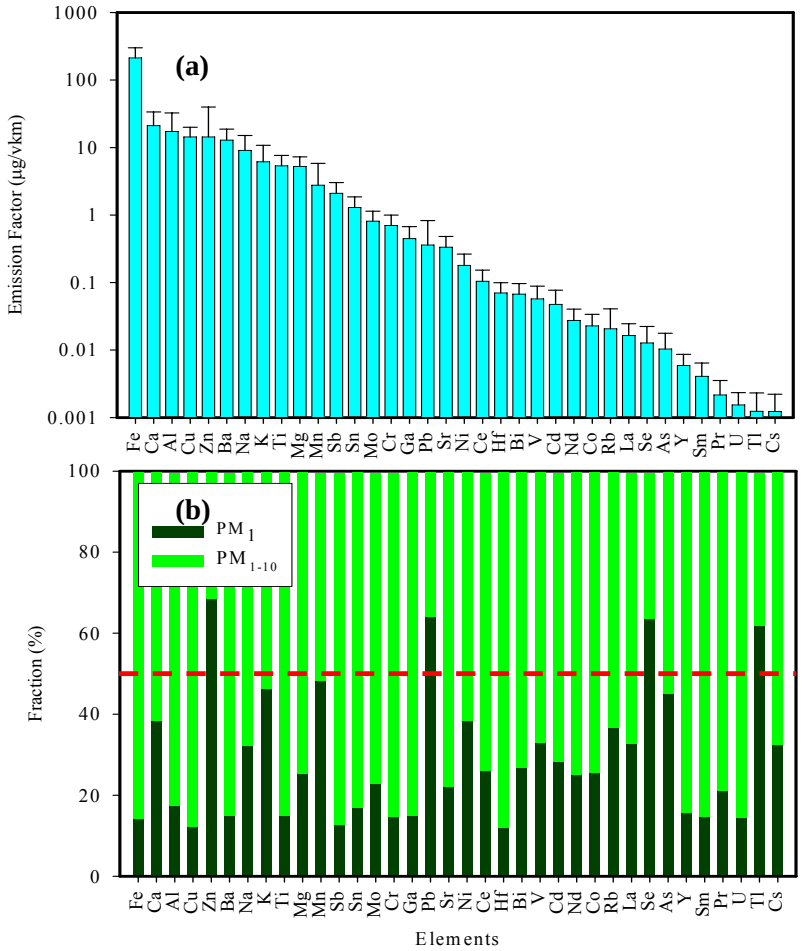

Figure 6. (a) Average (mean $\pm 1\sigma$) EmFs ($\mu g\,vkm^{-1}$) of trace metals in PM_{10} and **(b)** their partition in PM_1 and PM_{1-10} observed in Hsuehshan Tunnel. The red line indicates 50 %.

ACPD
14, 13963–14004, 2014

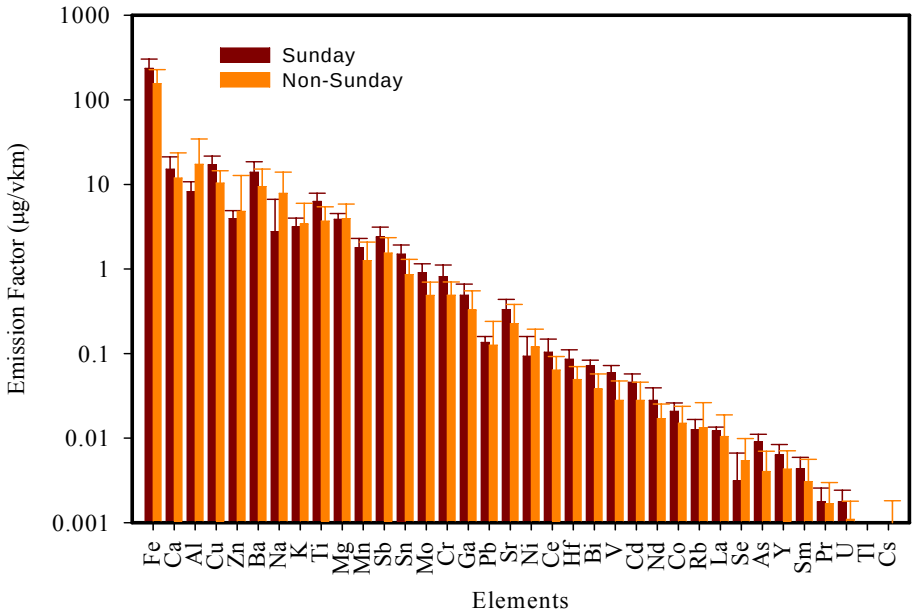

Figure 7. Comparison of emission factors (μg vkm^{-1}) of trace metals in PM_{1-10} between Sunday and non-Sunday samples collected in Hsuehshan Tunnel.

ACPD
14, 13963–14004, 2014